

Unconventional polaronic ground state in superconducting LiTi_2O_4

Zubia Hasan,^{1,*} Grace A. Pan,^{1,*} Harrison LaBollita,² Austin Kaczmarek,³
Suk Hyun Sung,⁴ Shekhar Sharma,² Purnima P. Balakrishnan,⁵ Edward
Mercer,^{6,7} Vivek Bhartiya,⁸ Zaher Salman,⁹ Thomas Prokscha,⁹ Andreas Suter,⁹
Alexander J. Grutter,⁵ Mirian Garcia-Fernandez,¹⁰ Ke-Jin Zhou,¹⁰ Jonathan
Pelliciari,⁸ Valentina Bisogni,⁸ Ismail El Baggari,⁴ Darrell G. Schlom,^{11,12}
Matthew R. Barone,¹¹ Charles M. Brooks,¹ Katja C. Nowack,³ Antia S.
Botana,² Brendan D. Faeth,¹¹ Alberto de la Torre,^{6,7,†} and Julia A. Mundy^{1,†}

¹*Department of Physics, Harvard University, Cambridge, MA, USA*

²*Department of Physics, Arizona State University, Tempe, AZ, USA*

³*Laboratory of Atomic and Solid-State Physics,
Cornell University, Ithaca, NY, USA*

⁴*The Rowland Institute, Harvard University, Cambridge, MA, USA*

⁵*NIST Center for Neutron Research,
National Institute for Standards and Technology, Gaithersburg, MD, USA*

⁶*Department of Physics, Northeastern University, Boston, MA, 02115, USA*

⁷*Quantum Materials and Sensing Institute,
Northeastern University, Burlington, MA, 01803 USA*

⁸*National Synchrotron Light Source II,
Brookhaven National Laboratory, Upton, NY 11973, USA*

⁹*PSI center for Neutron and Muon Sciences, 5232 Villigen PSI, Switzerland*

¹⁰*Diamond Light Source, Harwell Campus, Didcot OX11 0DE, UK.*

¹¹*Platform for the Accelerated Realization, Analysis,
and Discovery of Interface Materials (PARADIM),
Cornell University, Ithaca, NY, USA*

¹²*Department of Materials Science and Engineering,
Cornell University, Ithaca, New York 14853, USA*

(Dated: June 11, 2025)

* These authors contributed equally to this work.

† Correspondence should be addressed to: a.delatorreduran@northeastern.edu; mundy@fas.harvard.edu

Geometrically frustrated lattices can display a range of correlated phenomena, ranging from spin frustration and charge order to dispersionless flat bands due to quantum interference. One particularly compelling family of such materials is the half-valence spinel LiB_2O_4 materials. On the B -site frustrated pyrochlore sublattice, the interplay of correlated metallic behavior and charge frustration leads to a superconducting state in LiTi_2O_4 and heavy fermion behavior in LiV_2O_4 . To date, however, LiTi_2O_4 has primarily been understood as a conventional BCS superconductor despite a lattice structure that could host more exotic groundstates. Here, we present a multimodal investigation of LiTi_2O_4 , combining ARPES, RIXS, proximate magnetic probes, and ab-initio many-body theoretical calculations. Our data reveals a novel mobile polaronic ground state with spectroscopic signatures that underlie co-dominant electron-phonon coupling and electron-electron correlations also found in the lightly doped cuprates. The cooperation between the two interaction scales distinguishes LiTi_2O_4 from other superconducting titanates, suggesting an unconventional origin to superconductivity in LiTi_2O_4 . Our work deepens our understanding of the rare interplay of electron-electron correlations and electron-phonon coupling in unconventional superconducting systems. In particular, our work identifies the geometrically frustrated, mixed-valence spinel family as an under-explored platform for discovering unconventional, correlated ground states.

The interplay between electron-electron correlations and electron-phonon coupling has been of long-standing interest in understanding superconductivity. In traditional Bardeen-Cooper-Schrieffer (BCS) superconductors, Coulomb repulsion between electrons is thought to screen electron-phonon coupling and reduce the superconducting transition temperature T_c ¹. In unconventional superconductors, however, there can be a more complex interplay between electron-phonon coupling and electron-electron interactions. Strong correlations can further strengthen the electron-phonon coupling and enhance T_c ²⁻⁴. In certain cases, as explored for cuprates⁵, the energy scales of strong electron-electron correlations can overwhelm those of electron-phonon interactions, leading to charge and spin fluctuations that compete with or enhance superconductivity⁶. Thus, understanding how electronic correlations and electron-phonon coupling interact in superconductors is important in identifying new families of unconventional superconductors and ascertaining the mechanisms behind

high temperature superconductivity.

Although superconductivity was discovered in LiTi_2O_4 before the cuprates⁷, it remains a unique instance of a spinel superconductor and with the highest T_c for a mixed-valence titanate. In this crystal structure, $d^{0.5}$ titanium atoms form a pyrochlore sublattice, comprised of alternating planes of Kagome and triangles (Fig. 1a and 1b). This geometric construction can give rise to flat bands due to quantum interference, which has led to strong electron correlations in other systems⁸. Still, superconductivity in LiTi_2O_4 has primarily been considered as phonon-mediated BCS-like supported by specific heat, tunneling spectroscopy, and muon spin rotation measurements⁹⁻¹¹. In contrast, anomalous magnetotransport behavior and scanning tunneling spectroscopy experiments have suggested the presence of spin fluctuations, orbital ordering, and pseudo-gap like states in LiTi_2O_4 , all of which are typically associated with unconventional superconductors and strongly correlated materials^{10,12,13}. Interestingly, previous theoretical studies of LiTi_2O_4 have suggested non-BCS-like superconducting mechanisms, such as bipolaronic^{14,15} or resonating valence bond (RVB) superconductivity^{16,17}. While there have been speculations about the role of electron-electron correlations^{9,18}, a more detailed investigation into the strength and nature of various correlations is needed to explore the notion of "unconventional superconductivity" in LiTi_2O_4 .

Here, we reveal the complex interplay between electron-phonon coupling and electron-electron interactions in LiTi_2O_4 . We use molecular-beam epitaxy (MBE) to synthesize epitaxial thin films of superconducting LiTi_2O_4 , enabling a detailed spectroscopic investigation using resonant inelastic x-ray scattering (RIXS) and angle-resolved photoemission spectroscopy (ARPES). The combination of the element-specific sensitivity to structural and local excitations of RIXS together with the unique capability of ARPES to reveal energy and momentum dependence of the quasiparticle self-energy enable us to provide a comprehensive description of the low energy physics of LiTi_2O_4 . We observe evidence of strong electronic correlations and signatures of strong electron-phonon coupling. The cooperation between these two interaction scales gives rise to a novel polaronic ground state - also found in weakly doped cuprates¹⁹ - that dynamically localizes titanium states in LiTi_2O_4 . This interpretation is further supported by our theoretical calculations, which can reproduce some of the spectral features in our ARPES data when considering electron correlations or electron-phonon interactions separately but are unable to reproduce polaronic phenomena

associated with the interplay of both interactions. Our work thus challenges the notion of phonon-dominated BCS superconductivity in LiTi_2O_4 by revealing the complex correlations present in this material, hearkening comparisons to cuprate-like physics.

Results

Synthesis and characterization of superconducting LiTi_2O_4

Thin films of LiTi_2O_4 were grown via reactive oxide MBE on (111)-oriented MgAl_2O_4 substrates (see Methods). As shown in Fig. 1c, the films display a superconducting transition with $T_c \sim 12.5$ K and a residual resistivity ratio (RRR) of ~ 5.3 (Fig. S3) consistent with previous reports of the highest quality materials^{7,10}. Figure 1d,e show high-angle annular dark field scanning transmission electron microscopy (HAADF-STEM) images of LiTi_2O_4 , attesting to the high structural quality of our films (also see Supp. Fig. S1).

Additionally, we confirm the onset of superconductivity and probe the superconducting order parameter using scanning superconducting quantum interference device (SQUID) microscopy, which locally measures magnetic susceptibility (Fig. S4). The measured magnetic susceptibility can be used to extract the temperature dependence of the reduced London penetration depth (Supp. Mat. Sec. S3), which can be well-fit by a fully gapped order parameter, consistent with *s*-wave-like pairing. The observation of the 2-D thin film limit of superconductivity, the high RRR, as well as a homogeneous diamagnetic response from scanning SQUID demonstrates the high structural quality of our films, ensuring that further measurements probe the intrinsic behavior of LiTi_2O_4 .

Electron-electron correlations in LiTi_2O_4

Poised with high-quality thin films, we first probe the electronic structure using elemental-specific RIXS measurements. Figure 2a shows the RIXS intensity of LiTi_2O_4 near the Ti-L_3 edge. Our x-ray absorption spectroscopy (XAS) data (Fig. S13), displays resonant features associated with the mixed valence Ti^{4+} and Ti^{3+} states. Given the nearly featureless RIXS spectrum expected from a d^0 state²⁰, we conclude that the RIXS map in Fig. 2a, reflects a d^1 titanium occupation state, which given the lack of charge order in LiTi_2O_4 can only be dynamically populated²¹. Our RIXS data is characterized by broad Raman-like features centered at $E_{\text{loss}} = 1.5$ eV and $E_{\text{loss}} = 4$ eV. These excitations, along with the suppressed

fluorescence contribution, are unexpected, given that the itinerant charge carriers in our metallic and superconducting samples are proposed to have a dominant Ti-3*d* band character near the Fermi level^{22,23}. We note that our RIXS data resembles that of MgTi₂O₄²⁴ despite LiTi₂O₄ lacking large static local trigonal distortions of the TiO₆ octahedra and Ti-Ti dimerization (Supp. Fig. S1 and Supp. Fig. S17). The qualitative similarities between the RIXS energy maps in metallic LiTi₂O₄ and Mott-insulating systems like MgTi₂O₄ are suggestive of the presence of localized excitations in LiTi₂O₄.

In addition to the Raman-like excitations, we observe spectral weight associated with a fluorescence contribution with a linear dispersion in E_i that extends below $E_{loss} \leq 1.5$ eV. This resembles the superposition of localized and delocalized excitations observed in negative charge transfer insulators²⁵. Moreover, O-*K*-edge RIXS, shown in Fig. 2b, also shows Raman-like and fluorescence contributions below the charge transfer gap, $\Delta \approx 4.5$ eV. This is the same energy as the intra-*dd* excitations at the Ti-*L*₃ edge, suggesting strong hybridization between titanium and oxygen carriers. While the hybridization between Ti-3*d* and O-2*p* states has been previously theorized²², the RIXS data is the first instance of direct observation of strong titanium-oxygen hybridization. Moreover, the presence of fluorescence contributions at the O-*K*-edge near the elastic line (zero energy loss) suggests a larger contribution of oxygen carriers to electronic transport in LiTi₂O₄ than that expected from previous density of states (DOS) calculations²². Thus, our RIXS data suggest the presence of charge localization, Ti-3*d* and O-2*p* hybridization, and electron-electron correlations in LiTi₂O₄.

Electron-electron correlations are also observed in *in-situ* ARPES measurements on LiTi₂O₄. Figure 2c shows the Fermi surface of LiTi₂O₄ from our ARPES measurements. Here, k_x and k_y are chosen to lie along the $[11\bar{2}]$ and $[\bar{1}10]$ directions respectively. The Fermi surface is characterized by large electron pockets with hexagonal symmetry centered at Γ , pushing toward the zone boundary in proximity to a Lifshitz transition, which has led to enhanced electronic interactions near the Fermi surface for other superconductors²⁶. A more detailed discussion of the Fermi surface and its k_z dependence is given in Supp. Fig. S5, S6 and in the Supp. Mater. Sec S4.

To analyze the electronic interactions, we look at high-symmetry cuts of the band structure of LiTi₂O₄. In Fig. 2d,e, we compare our experimental band structure along $\bar{\Gamma} - \bar{K}$ to the momentum-resolved spectral function obtained from density-functional theory plus

dynamical mean-field theory (DFT+DMFT). The non-interacting band dispersion is shown in white in Fig. 2e for reference. The DFT+DMFT calculation reproduces the experimental dispersion near Γ , capturing the large effective mass renormalization compared to the bare DFT band – a clear indication of strong electron correlations in LiTi_2O_4 . The calculated cyclotron mass (Supp. Mater. Fig. S9) yields $\frac{m_{eff}}{m_{bare}} = 2.53 \pm 0.4$. This method of calculating the renormalization agrees with previous reports of the effective mass of LiTi_2O_4 by other optical probes^{27,28}. Additionally, we observe a broad Gaussian-like, intense incoherent spectral weight centered at $E_B \approx 0.9$ eV that resembles the lower Hubbard band of lightly doped cuprates²⁹. Intriguingly, the spectral weight disappears in the data taken by Ne-I α photon energy (16.85 eV), but the “water-fall” like features remain (Supp. Fig. S6). We note this feature cannot be reproduced by DMFT calculations but is consistent with a previous photoemission spectroscopy measurement of LiTi_2O_4 , where it was interpreted as a signature of polaronic behavior¹⁴. Nonetheless, our combined ARPES and RIXS data provide the first observation of significant electronic correlations in LiTi_2O_4 .

Electron-phonon coupling in LiTi_2O_4

While electronic correlations are important for unconventional superconductivity, we also observe signatures of electron-phonon coupling in the electronic structure of LiTi_2O_4 . Consistent with previous ARPES reports³⁰, we observe a ‘kink’ at $E_B \approx 46$ meV as shown in Fig. 3a. This feature is ascribed to an E_g oxygen phonon mode by tunneling spectroscopy measurements³¹ and inelastic neutron scattering³², confirmed by calculations of the spectral function including the self-energy from only electron-phonon interactions (Supp. Mat. Sec. S5). We extract a band renormalization, $\lambda_{tot} = 1.80(1)$ three times higher than $\lambda_{e-ph} = 0.65$ determined by specific heat measurements⁹ and ab-initio calculations¹⁸. The extracted band renormalization value from our ARPES data is comparable to that from electronic specific heat measurements, where the larger value is attributed to enhancement from electron-electron correlations or spin fluctuations^{23,33,34}. For a more detailed discussion on the calculation of λ_{tot} as well as its temperature and momentum dependence, see Sec. Mater. Sec S4 and Fig. S7.

Figure 3b shows an energy-momentum cut along the $\bar{\Gamma} - \bar{K} - \bar{M}$ direction (cut overlaid on the Brillouin zone is shown in Fig. S8a). Here we observe incoherent spectral weight at

$E_B = 46 \pm 10$ meV at all $k_{||}$. To examine this non-dispersive feature, we present two energy dispersive cuts (EDC) in Fig. 3c, k_{EDC1} which cuts across momentum value devoid of bands and k_{EDC2} which cuts across the k_F of the main LiTi_2O_4 band. The momentum position of these two cuts are indicated by two black arrows pointing to dotted white lines in Fig. 3b. We can see the distinct signature of this flat feature in the EDC of k_{EDC1} as an abrupt and sharp increase in spectral intensity at $\Omega = 46 \pm 10$ meV (green dot) also observed in k_{EDC2} at the same energy scale. These observations contrast the expected EDC for a non-interacting picture where, in the absence of bands, we would not expect any additional poles in the EDC, unlike what is seen at k_{EDC1} . The second derivative plot (Fig. 3c) highlights this feature and additionally shows a “spectral gap” where the flat feature interrupts the main band electron pocket. We note that the flat feature, in addition to the spectral gap, can also be seen clearly in our raw data in Fig. 2d. Spectral signatures such as these are consistent with the formation of intra-unit cell small polarons³⁵ that have been observed in other correlated materials^{36,37}.

Our RIXS measurements also corroborate the presence of strong electron-phonon coupling and multiphonon processes in LiTi_2O_4 . Figure 3e shows the RIXS spectra at the Ti- L_3 and O- K edge, respectively. As highlighted by black arrows in Fig. 3e and f, both RIXS spectra are characterized by prominent quasi-elastic peaks that are approximately equally spaced and monotonically decay with E_{loss} , thus resembling the harmonic progression of the multiphononic processes. The low-energy excitations shown in the titanium spectra are well fit by the Ament model³⁸, which considers a single non-dispersive phonon mode coupled to the electronic structure with strength g (See Supp. Mater. Sec S6 for more details on the Ament model fit). At the Ti- L_3 edge, the Ament model in conjunction with a broad Gaussian peak centered at $E_{loss} = 90$ meV provides a good fit for a mode centered at $\Omega = 47 \pm 2$ meV, in agreement with the oxygen E_g mode observed in ARPES. We interpret this broad Gaussian peak to represent multiple incoherent phononic excitations that cannot be resolved within the energy resolution of the instrument, also observed in MgTi_2O_4 ²⁴.

The coupling strength, $g_{Ti} = 9.1 \pm 3.0$, far exceeds those of other titanates^{39,40}, and is on par with some cuprates measured via RIXS⁴¹ further supporting strong electron-phonon coupling in LiTi_2O_4 . Moreover, the observation of a pure oxygen E_g mode at the titanium edge is indicative of strong hybridization between the O-2p and the Ti-3d orbitals. Similar to the Ti- L_3 edge, the three excitations at the O- K edge can also be well fit by the Ament

model in conjunction with a broad Gaussian peak. The fit gives us the first three harmonics of a phonon mode centered at $\Omega = 71 \pm 1$ meV with $g_O = 6.89 \pm 3.17$. We assign this mode to the oxygen A_{1g} phonon, which is known to be strongly coupled to the E_g mode¹⁸. We note that our DFT calculations of the phonon band structure (Fig. 3g) show the modes around $\Omega \approx 46$ meV and ≈ 75 meV to be relatively nondispersive, supporting our choice of Ament model fitting for the quasi-elastic peaks at the Ti- L_3 and O- K edge.

Discussion

Our combined spectroscopic data indicates that the effects of electron-electron correlations and electron-phonon coupling cannot be disentangled in LiTi_2O_4 . Moreover, *ab-initio* calculations (Fig. 2e and Fig. 3a) treating electron-phonon coupling and electron-electron correlations separately fail to capture the most salient features of our data, namely the existence of localized excitations in LiTi_2O_4 (Fig. 2a) and the presence of a second pole in the photoemission self-energy (Fig. 3c). While the combined theoretical description of these two energy scales remains challenging and a matter of active research⁴², there is growing evidence that the excitation spectrum, band structure and transport properties of quantum materials such as SrVO_3 ⁴³ and superconductors like alkali-fullerides³⁷ and the cuprates⁴⁴ can only be understood through the interplay of both interaction scales. We note that while competing interactions is generally associated with unconventional superconductivity, our scanning SQUID data is consistent with a conventional s-wave order parameter (Supp. Sec. S3). This naturally also raises the question as to how the phonon - mediated attractive interaction - essential for s-wave superconductivity - is robust against or potentially enhanced by the repulsive electronic correlations apparent in LiTi_2O_4 . Within this context, LiTi_2O_4 departs from SrTiO_3 ⁴⁵ and other superconducting titanates^{46,47} where electron-phonon coupling is understood to be the dominant interaction.

We finally comment on the possible mechanism that enables the strong interplay of electron-electron and electron-phonon interactions in LiTi_2O_4 . In this context, it is instructive to consider the $d^{0.5}$ occupation state in LiTi_2O_4 in the context of the d^1 member of the AB_2O_4 family, MgTi_2O_4 . In MgTi_2O_4 , a trigonal distortion driven by E_g and A_{1g} oxygen phonons⁴⁸ lifts the orbital degeneracy of the Ti $3d^1$ state in a perfect cubic octahedral environment (Fig. 4 a, b). The combination of this local distortion with the formation of Ti-Ti dimers at $T = 260$ K⁴⁸ leads to a tetragonal, dimerized unit cell and the formation

of a correlated insulating state (Fig. 4b) in MgTi_2O_4 . In the $d^{0.5}$ mixed-valence state the energy gain from dimerization is reduced in favor of a charge-ordered ground state, such as in mixed-valence spinel CuIr_2S_4 ⁴⁹. However, no static symmetry breaking due to orbital or lattice ordering has been reported in LiTi_2O_4 ¹⁰, possibly due to the geometric frustration inherent in the spinel structure. This raises the question of how the d^1 state, with its associated local distortion, is accommodated in LiTi_2O_4 . We speculate that in LiTi_2O_4 with an occupation $d^{0.5}$ in the absence of charge order, two titanium ions share an electron dynamically, such that their occupation state fluctuates between d^1 and d^0 . In this scenario, the transiently occupied d^1 site has an associated local symmetry reduction due to dynamic lattice fluctuations of the E_g and A_{1g} oxygen phonons, as seen in MgTi_2O_4 ⁵⁰. As the electron moves to the unoccupied d^0 site, it drags the local distortion with it, leading to the formation of a polaronic state in which charge motion and lattice distortions are coupled (Fig. 4b).

Our data reflects the formation of such a small mobile polaronic state in LiTi_2O_4 . First, our ARPES data shows a strong coupling ($\lambda > 1$) to a non-dispersive E_g phonon mode. The ratio of the dominant E_g phonon mode energy ($\Omega = 46$ meV), to the bare electron bandwidth ($t \approx 800$ meV), places LiTi_2O_4 in the adiabatic limit ($\Omega/t \ll 1$) for which the condition $\lambda > 1$ is expected for a small polaron ground state⁵¹. Second, the observation of the same mode (E_g oxygen mode) at the $\text{Ti-}L_3$ edge indicates a tightly hybridized state between the localized d^1 titanium electrons and the deformed lattice. Third, we observe large incoherent spectral weight at $E = 800$ meV, which cannot be accounted by either of our density-functional perturbation theory (DFPT) or DMFT calculations. We note that polaronic behavior has been previously discussed for LiTi_2O_4 based on the anomalous transport behavior of off-stoichiometric samples⁵² and previous photoemission and reflectance spectroscopy data^{14,53}. Notably, the metallic behavior of LiTi_2O_4 at all temperatures contrasts with the localized small Holstein polaron behavior of other titanates^{54,55} where a low-temperature insulating state occurs due to reduced lattice mobility. However, in the light regime ($m^* < 10m$), small polarons have been theoretically predicted to be mobile^{56,57}. Polaron delocalization involves a crawling-like motion in which an electron is transiently delocalized over two neighboring sites⁵⁸, similar to the mechanism suggested here for the $d^{0.5}$ state in LiTi_2O_4 (Fig. 4b) in which the dynamical lattice fluctuations are coupled to electron hopping between d^1 and d^0 states. We note that this mobile polaron formation requires an intricate balance between

electron-electron correlations and electron-phonon coupling. Dominant electron-electron correlations may choose a charge-ordered ground state⁴⁹ while dominant electron-phonon coupling can lead to bi-polaron formation as suggested for other titanates, like Ti_4O_7 ⁵⁵. Thus, our data suggests a serendipitous balancing of electron-electron correlations with electron-phonon coupling in this material.

Although LiTi_2O_4 has long been thought of as a well-studied BCS superconductor consistent with phonon-dominated superconductivity as in other titanates^{46,47} - our work forces us to reconsider the notion of conventional superconductivity in LiTi_2O_4 . Here, a re-examination of LiTi_2O_4 using ARPES and RIXS measurements uncovers strong hybridization between titanium and oxygen, considerable electron-electron correlations, and co-existing electron-phonon coupling. In mixed valence LiTi_2O_4 , this balance of energy scales results in a novel mobile polaronic ground state indicative of a unique balance of charge delocalization, electron-electron correlations, and electron-phonon coupling. LiTi_2O_4 becomes a model system to explore predictions of enhancement of superconductivity due to the cooperative effect of electron-electron correlations and electron-phonon coupling in the quarter-filled Hubbard Hamiltonian⁵⁹. Moreover, the proximity of superconductivity to an orbitally ordered phase, the correlated behavior, and the strong hybridization between titanium and oxygen highlights a rich competition between energy scales found only in special classes of quantum materials. Our work expands our understanding of superconductivity in $d^{0.5}$ systems and demonstrates how mixed-valence spinel-oxide structures can host correlated physics, thus broadening our search of material families that can host such correlated phenomena.

Acknowledgements

We thank useful discussions with G. Grissonnanche, M. R. Norman, Y. Wang, F. Baumberger, and J. Sous. This research is primarily supported by the National Science Foundation, Division of Materials Research, under Award No. DMR-2339913. Materials growth and photoemission studies were supported by the Platform for the Accelerated Realization, Analysis, and Discovery of Interface Materials (PARADIM) under NSF Cooperative Agreement No. DMR-2039380. All nanofabrication work was performed at Harvard University's Center for Nanoscale Systems (CNS), a member of the National Nanotechnology Coordinated Infrastructure Network (NNCI), supported by the National Science Foundation under NSF Grant No. 2025158. Z.H. and G.A.P. acknowledge support from the Paul & Daisy Soros Fellowship for New Americans. G.A.P. acknowledges additional support from the NSF Graduate Research Fellowship Grant No. DGE-1745303. A.K. and K.C.N. acknowledge support from the Air Force Research Laboratory, Project Grant FA95502110429. S.H.S. and I.E.B. acknowledge support from the Rowland Institute at Harvard University. J.A.M. acknowledges support from the Packard Foundation and the Sloan Foundation. This research used beamline 2-ID of the National Synchrotron Light Source II which is a US DOE Office of Science Facility operated for the DOE Office of Science by Brookhaven National Laboratory under contract no. DE-SC0012704. HL and ASB acknowledge support from NSF Grant No. DMR-2323971. The μ SR experiments were performed at the Swiss Muon Source, S μ S, Paul Scherrer Institute, Villigen, Switzerland.

Author Contributions

Z.H., G.A.P., C.M.B. and J.A.M. synthesized the thin films with assistance from M.R.B and D.G.S. Electrical transport measurements were performed and analyzed by G.A.P. Scanning transmission electron microscopy was performed by S.H.S. and I.E. ARPES measurements were performed by Z.H., G.A.P. and B.D.F. ARPES analysis was done by Z.H. and B.D.F. with support by A.d.l.T. The RIXS measurements were performed by Z.H., E.M., S.H.S., I.B. and A.d.l.T. with support from V.B., V.B. and J.P. and M.G.F. and K.Z. RIXS analysis was done by Z.H., S.H.S and E.M under the supervision of A.d.l.T. μ SR measurements were performed by A.J.G and P.P.B with support from A.S., Z.S., T.P. Analysis of μ SR data was done by A.J.G and P.P.B. Scanning SQUID measurements were performed by A.K. and

K.C.N. H.L, S.S. and A.S.B performed the DFT, DMFT, and electron-phonon calculations. J.A.M. and A.d.l.T. conceived and guided the study. Z.H., G.A.P., J.A.M., and A.d.l.T. wrote the manuscript with contributions and discussion from all authors.

Competing Interests

The authors declare no competing interests.

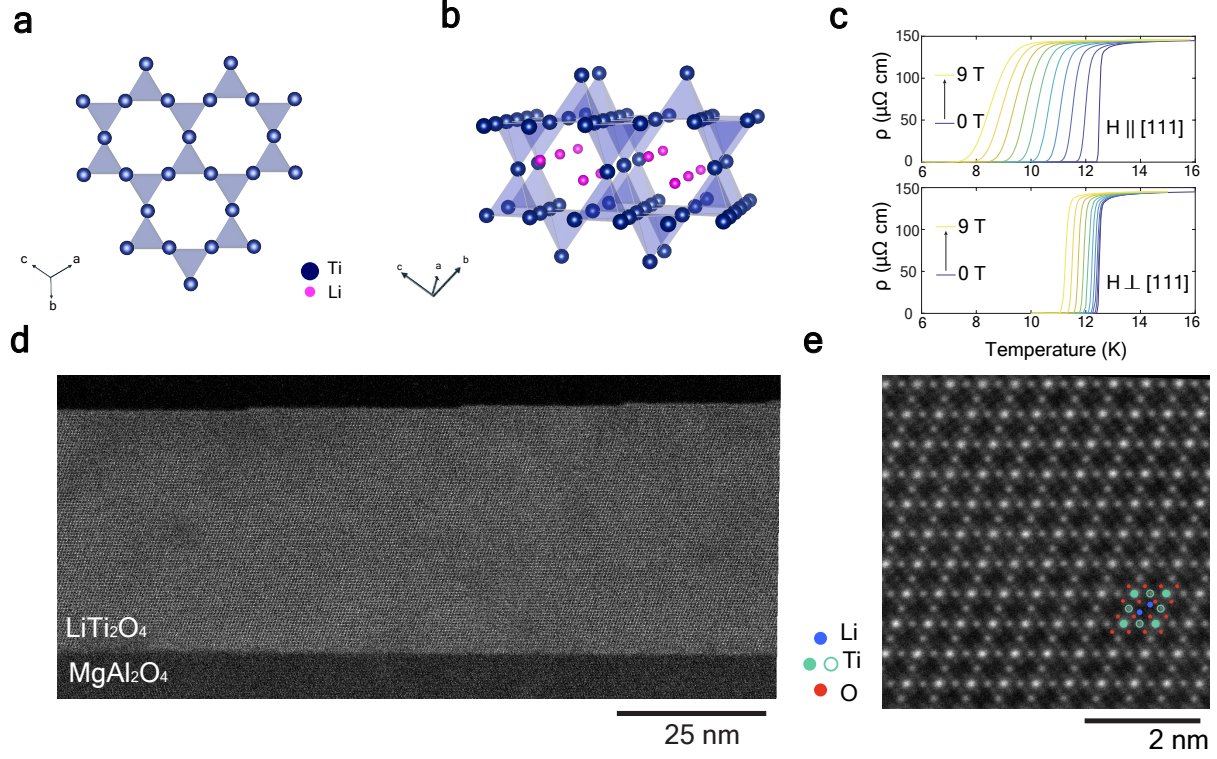


FIG. 1. **Structural and electrical characterization of LiTi_2O_4** **a**, The (111) plane of LiTi_2O_4 showing the titanium kagome sublattice inherent to the spinel structure. **b**, Side-view of the (111) plane shown in **a**, highlighting the three-dimensional nature of the geometric frustration in LiTi_2O_4 . **c**, Resistivity ρ vs temperature of LiTi_2O_4 with magnetic field (0 to 9 T) parallel and perpendicular to the sample. **d**, zoomed out HAADF-STEM image of LiTi_2O_4 showing uniform crystallinity over a large area. **e**, Zoomed-in HAADF-STEM image of LiTi_2O_4 overlaid with the corresponding atoms.

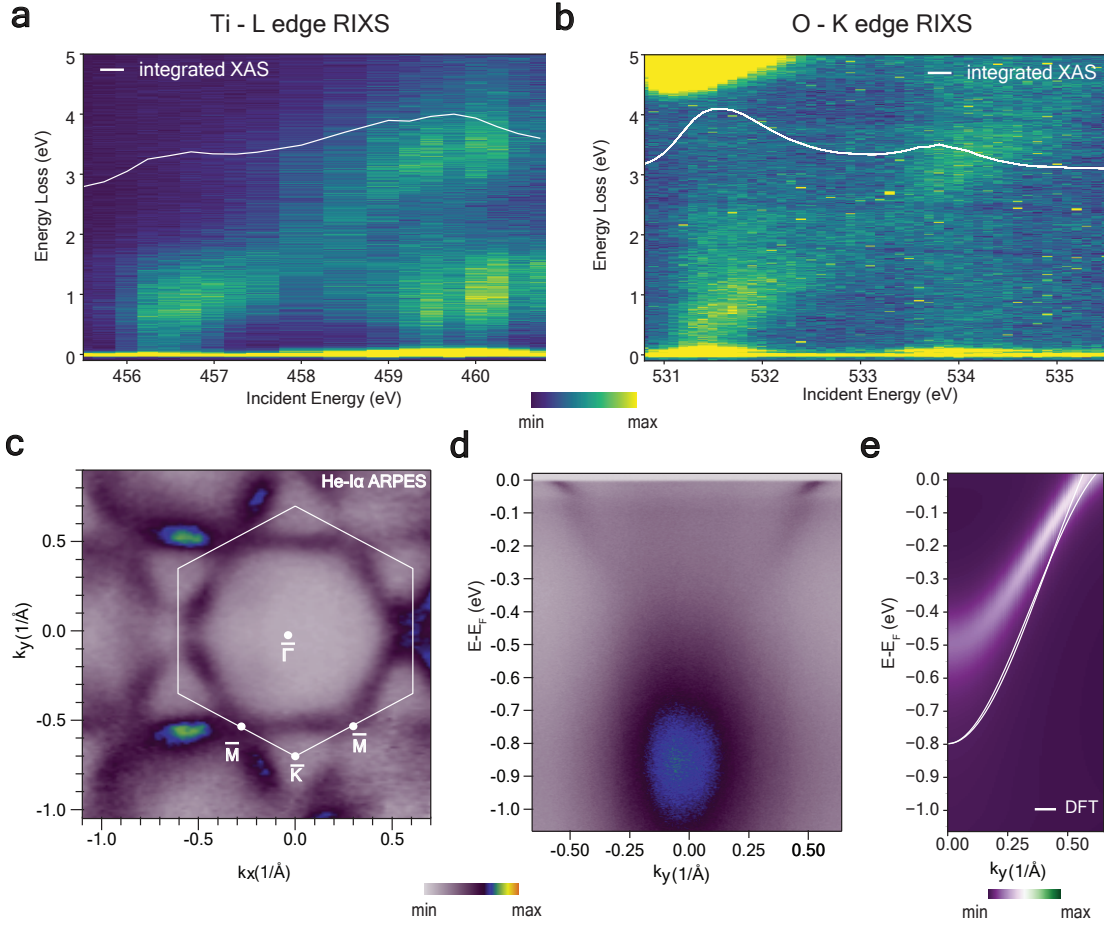


FIG. 2. **Electron-electron correlations in LiTi_2O_4** **a**, RIXS intensity at the Ti-L_3 edge. **b**, RIXS intensity at the O-K edge. **c**, Iso-energy map at the Fermi level taken with $\text{He-I}\alpha$ showing a hexagonal Fermi surface. The white hexagon indicates the first Brillouin zone. **d**, Experimental band structure in the $\bar{K} - \bar{\Gamma} - \bar{K}$ direction. **e**, DMFT and DFT (white) comparison along $\bar{\Gamma} - \bar{K}$ indicating the mass renormalization due to electron-electron correlations.

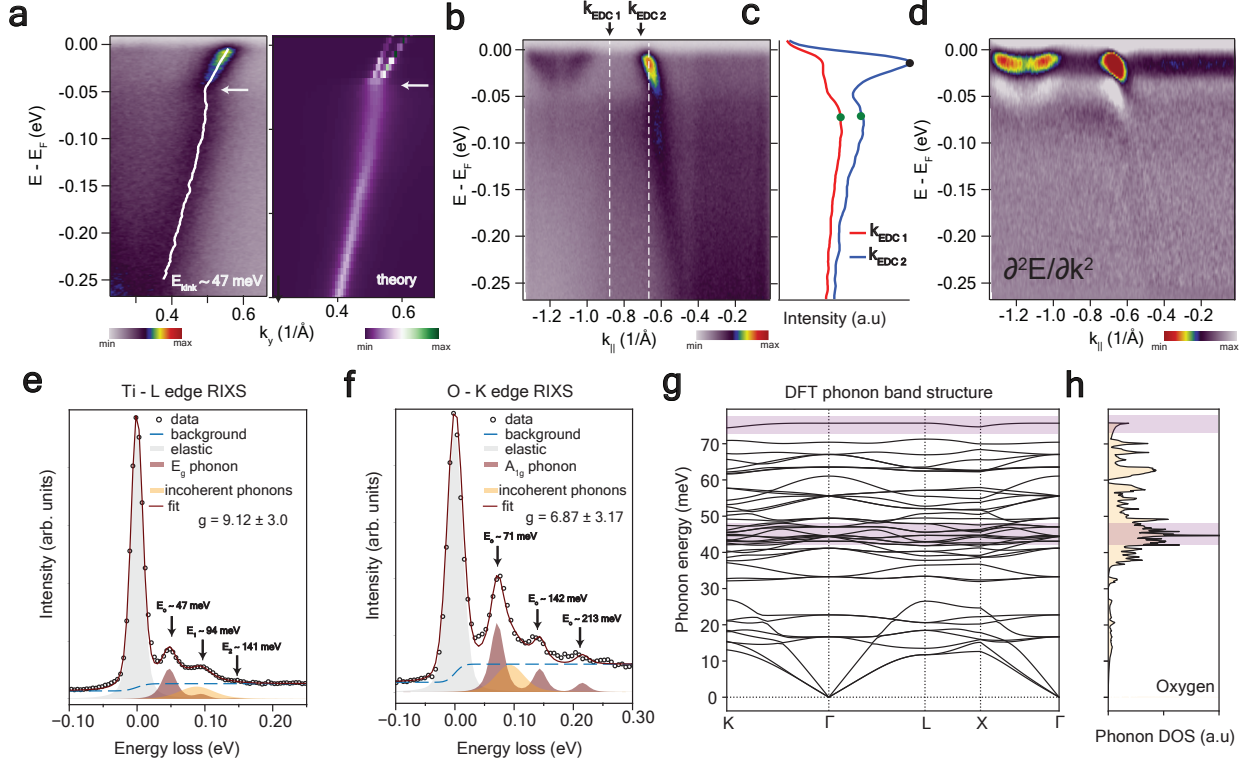


FIG. 3. Electron-phonon coupling in LiTi_2O_4 **(a)** Comparison of the $\bar{\Gamma} - \bar{K}$ ARPES data to density-functional perturbation theory (DFPT) highlighting the kink feature at 47 meV at $\bar{\Gamma} - \bar{K}$ at $T = 7$ K. **(b)** Energy - momentum ARPES spectra along the $\bar{\Gamma} - \bar{K} - \bar{M}$ direction. **(c)** EDC cuts at two different $k_{||}$ highlighted in **(b)** with dotted white lines. Black and green dots correspond to the top of the two EDC poles. **(d)** Second-derivative plot from **(b)**, highlighting a dispersionless spectral intensity at the second pole denoted by a black arrow in **(c)** also observable in the raw data in **(b)**. A spectral gap is also prominent at the same energy scale where the dispersionless feature interrupts the main band. **(e)** Quasi-elastic RIXS excitations shown at $E_{inc} = 460$ eV for the Ti- L_3 edge. **(f)** Quasi-elastic RIXS excitations shown at $E_{inc} = 531.5$ eV for the O- K edge. The total intensity is a fit (red solid line) to a Voigt peak (grey shading), a background step function (blue dashed lines), and Ament Model fit to the phonon spectra (maroon) in **(e)** and **(f)**. **(g)** and **(h)**, Calculated phonon band structure and total oxygen phonon density of states respectively. The purple boxes highlights the energy scale of the A_{1g} and E_g modes, respectively, in both plots.

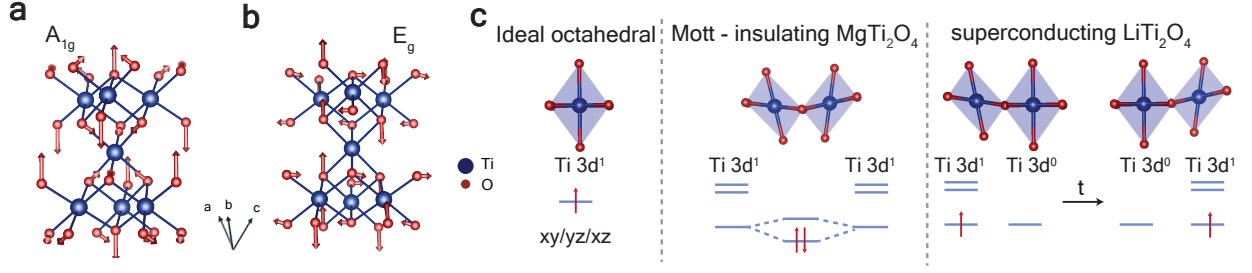


FIG. 4. **Polaron formation in LiTi_2O_4 .** **a,b**, DFT calculated A_{1g} and E_g oxygen phonon modes in LiTi_2O_4 . **c**, An ideal TiO_6 octahedra (left) with a highly degenerate d^1 state in a cubic crystal field. In MgTi_2O_4 , a local trigonal distortion driven by E_g and A_{1g} phonons is required to achieve a dimerized ground state (middle). Dynamic symmetry-reducing local lattice fluctuations associated with electron hopping leading to polaron formation in LiTi_2O_4 (right)

Methods

Synthesis of LiTi_2O_4 thin films via MBE

We used reactive oxide molecular beam epitaxy (Veeco GEN 10) to synthesize thin film LiTi_2O_4 on untreated MgAl_2O_4 (111) substrates (CrysTec GmbH). The lithium and titanium fluxes were matched and set to $\sim 1.5 \times 10^{13}$ atoms/cm²·s as measured by a quartz crystal microbalance (QCM). We obtained the lithium flux by flowing O_2 during the QCM process and forming Li_2O , as the low atomic mass of elemental lithium yields small frequency changes on the QCM below the detection sensitivity except for at very high fluxes. For the deposition process, we heated the substrates with a 10.6 μm CO_2 laser to 825 °C in a pressure of 1.0 - 2.0×10^{-7} molecular O_2 over a chamber background pressure of $\sim 5.0 \times 10^{-8}$. We co-deposited the lithium and titanium sources for one hour. After deposition, we shut off the O_2 flow to prevent oxidation of titanium to the 4+ state and cooled at a rate of 100°C/min.

Structural characterization

Annular dark field (ADF) STEM was performed on Thermofisher Scientific (TFS) Themis (operated at 200 keV, convergence semi-angle 18.9 mrad, ADF collection angle: 36–200 mrad). A small ADF inner collection angle was used to increase light element sensitivity. Electron transparent TEM samples were prepared using TFS Helios DualBeam FIB/SEM.

Transport measurements

We performed all electrical transport measurements in a Hall bar geometry using evaporated Cr/Au (7 nm/100 nm) contacts with the Hall channel defined by a diamond scribe along the [11-2] crystallographic direction of the MgAl_2O_4 (111) substrate. We loaded the samples in 9 T Dynacool Physical Property Measurement System (PPMS) and used AC lock-in techniques at ~ 15 Hz.

Resonant inelastic X-ray scattering

The XAS and RIXS spectra were collected at the SIX beamline at NSLS-II and the I21 beamline of Diamond Light Source. The Ti- L_3 edge was measured at SIX and I21, while the O- K edge spectra was acquired at I21. The Ti- L_3 energy map is collected at $2\theta = 150^\circ$,

while the O- K energy map is collected at $2\theta = 90^\circ$. All RIXS spectra are collected at $2\theta = 90^\circ$ at grazing incidence of $\theta = 20^\circ$ unless indicated otherwise. The energy resolution was fixed between 20 to 25 meV at both SIX and Diamond, respectively. All data was measured at a base temperature of 22 K at both beamlines.

Angle resolved photoemission spectroscopy

All *in situ* photoemission measurements were conducted by immediately transferring the samples through a UHV manifold ($P < 2 \times 10^{-9}$ Torr) to a measurement chamber immediately following film growth. ARPES measurements were taken with a Scienta Omicron DA30-L electron analyzer equipped with a Fermion Instruments BL1200s multi-gas discharge lamp using He-I photons at 21.2 eV, Ne-I photons at 16.85 eV, and He-II photons at 40.2 eV. The base pressure in the ARPES system is maintained during measurements at pressures lower than 5×10^{-11} Torr. ARPES measurements were performed at a temperature of 7 K and a nominal experimental energy resolution of 10 meV unless otherwise indicated.

Muon spin relaxation measurements

Low-energy muon spin-relaxation (LE- μ SR) measurements were done using the LEM instrument at the Swiss muon source. An applied field of 10 mT was applied transverse to the μ^+ s spin polarization direction. For more details on the μ SR measurements, refer to Supp. Mat. Sec. S7.

Data Availability

The data supporting the findings of this study are available from the corresponding authors upon reasonable request.

-
1. B. T. Matthias. Chapter V Superconductivity in the Periodic System. In C. J. Gorter, editor, *Progress in Low Temperature Physics*, volume 2, pages 138–150. Elsevier, January 1957.
 2. M. Capone, M. Fabrizio, C. Castellani, and E. Tosatti. Strongly Correlated Superconductivity. *Science*, 296(5577):2364–2366, June 2002. Publisher: American Association for the Advancement of Science.

3. Zhihong Yuan, Pengyu Zheng, Yiran Peng, Rui Liu, Xiaobo Ma, Guangwei Wang, Tianye Yu, and Zhiping Yin. Correlation-enhanced electron-phonon coupling and superconductivity in (Ba,K)SbO₃ superconductors. *Physical Review B*, 105(1):014517, 2022.
4. Yusuke Nomura, Shiro Sakai, Massimo Capone, and Ryotaro Arita. Unified understanding of superconductivity and mott transition in alkali-doped fullerenes from first principles. *Science advances*, 1(7):e1500568, 2015.
5. Douglas J Scalapino. A common thread: The pairing interaction for unconventional superconductors. *Reviews of Modern Physics*, 84(4):1383–1417, 2012.
6. Erik G. C. P. van Loon, Malte Rösner, Gunnar Schönhoff, Mikhail I. Katsnelson, and Tim O. Wehling. Competing Coulomb and electron–phonon interactions in NbS₂. *npj Quantum Materials*, 3(1):1–8, July 2018. Publisher: Nature Publishing Group.
7. DC Johnston. Superconducting and normal state properties of Li_{1+x}Ti_{2–x}O₄ spinel compounds. i. preparation, crystallography, superconducting properties, electrical resistivity, dielectric behavior, and magnetic susceptibility. *Journal of Low Temperature Physics*, 25:145–175, 1976.
8. Joshua P. Wakefield, Mingu Kang, Paul M. Neves, Dongjin Oh, Shiang Fang, Ryan McTigue, S. Y. Frank Zhao, Tej N. Lamichhane, Alan Chen, Seongyong Lee, Sudong Park, Jae-Hoon Park, Chris Jozwiak, Aaron Bostwick, Eli Rotenberg, Anil Rajapitamahuni, Elio Vescovo, Jessica L. McChesney, David Graf, Johanna C. Palmstrom, Takehito Suzuki, Mingda Li, Riccardo Comin, and Joseph G. Checkelsky. Three-dimensional flat bands in pyrochlore metal CaNi₂. *Nature*, 623(7986):301–306, November 2023. Publisher: Nature Publishing Group.
9. C. P. Sun, J.-Y. Lin, S. Mollah, P. L. Ho, H. D. Yang, F. C. Hsu, Y. C. Liao, and M. K. Wu. Magnetic field dependence of low-temperature specific heat of the spinel oxide superconductor LiTi₂O₄. *Physical Review B*, 70(5):054519, August 2004.
10. K. Jin, G. He, X. Zhang, S. Maruyama, S. Yasui, R. Suchoski, J. Shin, Y. Jiang, H. S. Yu, J. Yuan, L. Shan, F. V. Kusmartsev, R. L. Greene, and I. Takeuchi. Anomalous magnetoresistance in the spinel superconductor LiTi₂O₄. *Nature Communications*, 6(1):7183, May 2015. Publisher: Nature Publishing Group.
11. W. D. Wu, A. Keren, L. P. Le, G. M. Luke, B. J. Sternlieb, Y. J. Uemura, D. C. Johnston, B. K. Cho, and P. Gehring. Magnetic penetration depth in V₃Si and LiTi₂O₄ measured by μ SR. *Hyperfine Interactions*, 86(1):615–621, December 1994.

12. Yoshinori Okada, Yasunobu Ando, Ryota Shimizu, Emi Minamitani, Susumu Shiraki, Satoshi Watanabe, and Taro Hitosugi. Scanning tunnelling spectroscopy of superconductivity on surfaces of $\text{LiTi}_2\text{O}_4(111)$ thin films. *Nature Communications*, 8:15975, July 2017.
13. Huanyi Xue, Lijie Wang, Zhongjie Wang, Guanqun Zhang, Wei Peng, Shiwei Wu, Chun-Lei Gao, Zhenghua An, Yan Chen, and Wei Li. Fourfold symmetric superconductivity in spinel oxide $\text{LiTi}_2\text{O}_4(001)$ thin films. *ACS Nano*, 16(11):19464–19471, November 2022. Publisher: American Chemical Society.
14. P. P. Edwards, R. G. Egdell, I. Fragala, J. B. Goodenough, M. R. Harrison, A. F. Orchard, and E. G. Scott. A study of the spinel materials LiTi_2O_4 and $\text{Li}_{43}\text{Ti}_{53}\text{O}_4$ by photoelectron spectroscopy. *Journal of Solid State Chemistry*, 54(2):127–135, September 1984.
15. A. Alexandrov and J. Ranninger. Bipolaronic superconductivity. *Physical Review B*, 24(3):1164–1169, August 1981.
16. P. W. Anderson. The resonating valence bond state in La_2CuO_4 and superconductivity. *Science*, 235(4793):1196–1198, March 1987. Publisher: American Association for the Advancement of Science.
17. P. W. Anderson, G. Baskaran, Z. Zou, and T. Hsu. Resonating-valence-bond theory of phase transitions and superconductivity in La_2CuO_4 -based compounds. *Physical Review Letters*, 58(26):2790–2793, June 1987. Publisher: American Physical Society.
18. T. Oda, M. Shirai, N. Suzuki, and K. Motizuki. Electron-phonon interaction, lattice dynamics and superconductivity of an oxide spinel LiTi_2O_4 . *Journal of Physics: Condensed Matter*, 6(35):6997, August 1994.
19. K. M. Shen, F. Ronning, D. H. Lu, W. S. Lee, N. J. C. Ingle, W. Meevasana, F. Baumberger, A. Damascelli, N. P. Armitage, L. L. Miller, Y. Kohsaka, M. Azuma, M. Takano, H. Takagi, and Z.-X. Shen. Missing Quasiparticles and the Chemical Potential Puzzle in the Doping Evolution of the Cuprate Superconductors. *Physical Review Letters*, 93(26):267002, December 2004. Publisher: American Physical Society.
20. Andrey Geondzhian, Alessia Sambri, Gabriella M. De Luca, Roberto Di Capua, Emiliano Di Gennaro, Davide Betto, Matteo Rossi, Ying Ying Peng, Roberto Fumagalli, Nicholas B. Brookes, Lucio Braicovich, Keith Gilmore, Giacomo Ghiringhelli, and Marco Salluzzo. Large polarons as key quasiparticles in SrTiO_3 and SrTiO_3 based heterostructures. *Physical Review Letters*, 125(12):126401, September 2020.

21. Naoya Iwahara and Shouta Shikano. Vibronic excitations in resonant inelastic x-ray scattering spectra of K_2RuCl_6 . *Phys. Rev. Res.*, 5:023051, Apr 2023.
22. S. Massidda, Jaejun Yu, and A. J. Freeman. Electronic structure and properties of superconducting LiTi_2O_4 . *Physical Review B*, 38(16):11352–11357, December 1988.
23. Sashi Satpathy and Richard M. Martin. Electronic structure of the superconducting oxide spinel LiTi_2O_4 . *Physical Review B*, 36(13):7269–7272, November 1987.
24. Qizhi Li, Abhishek Nag, Xiquan Zheng, Fucong Chen, Jie Yuan, Kui Jin, Yi Lu, Ke-Jin Zhou, and Yingying Peng. Evolution of orbital excitations from insulating to superconducting MgTi_2O_4 films. *Physical Review B*, 107(12):L121108, March 2023.
25. Valentina Bisogni, Sara Catalano, Robert J Green, Marta Gibert, Raoul Scherwitzl, Yaobo Huang, Vladimir N Strocov, Pavlo Zubko, Shadi Balandeh, Jean-Marc Triscone, et al. Ground-state oxygen holes and the metal–insulator transition in the negative charge-transfer rare-earth nickelates. *Nature Communications*, 7(1):13017, 2016.
26. Xun Shi, ZQ Han, XL Peng, P Richard, Tian Qian, XX Wu, MW Qiu, SC Wang, JP Hu, YJ Sun, et al. Enhanced superconductivity accompanying a Lifshitz transition in electron-doped FeSe monolayer. *Nature communications*, 8(1):14988, 2017.
27. Takeo Ohsawa, Naoomi Yamada, Akichika Kumatani, Yoshitaka Takagi, Tohru Suzuki, Ryota Shimizu, Susumu Shiraki, Tsutomu Nojima, and Taro Hitosugi. Origin of optical transparency in a transparent superconductor LiTi_2O_4 . *ACS Applied Electronic Materials*, 2(2):517–522, February 2020. Publisher: American Chemical Society.
28. Minglin Zhao, Jing Xu, Qian Li, Kui Jin, Fuyang Cao, Youyou Hu, Yang Li, Ting Gou, and Jun Dai. Pseudo-dielectric functions, band-to-band transitions, and dielectric-related factors in a single-crystal LiTi_2O_4 thin film. *Optical Materials*, 142:114034, August 2023.
29. AE Myasnikova, EA Zhileeva, and DV Moseykin. Relaxation of strongly coupled electron and phonon fields after photoemission and high-energy part of ARPES spectra of cuprates. *Journal of Physics: Condensed Matter*, 30(12):125601, 2018.
30. Yuita Fujisawa, Anjana Krishnadas, Chia-Hsiu Hsu, Takahito Takeda, Sheng Liu, Markel Pardo-Almanza, Yukiko Obata, Dyon van Dinter, Kohei Yamagami, Guoqing Chang, et al. Imaging emergent exotic quasiparticle state in a frustrated transition metal oxide. *arXiv preprint arXiv:2306.06708*, 2023.
31. Keith Gilmore, Jonathan Pelliciari, Yaobo Huang, Joshua J. Kas, Marcus Dantz, Vladimir N.

- Strocov, Shigeru Kasahara, Yuji Matsuda, Tanmoy Das, Takasada Shibauchi, and Thorsten Schmitt. Description of Resonant inelastic x-ray scattering in correlated metals. *Physical Review X*, 11(3):031013, July 2021. Publisher: American Physical Society.
32. M A Green, M Dalton, K Prassides, P Day, and D A Neumann. Lattice vibrations of the superconducting oxide spinels. *Journal of Physics: Condensed Matter*, 9(49):10855–10865, December 1997.
 33. J. M. Heintz, M. Drillon, R. Kuentzler, Y. Dossmann, J. P. Kappler, O. Durmeyer, and F. Gautier. Superconductivity of LiTi_2O_4 and related systems. *Zeitschrift für Physik B Condensed Matter*, 76(3):303–309, September 1989.
 34. RW McCallum, DC Johnston, CA Luengo, and MB Maple. Superconducting and normal state properties of $\text{Li}_{1+x}\text{Ti}_{2-x}\text{O}_4$ spinel compounds. ii. low-temperature heat capacity. *Journal of Low Temperature Physics*, 25:177–193, 1976.
 35. Martin Hohenadler, Markus Aichhorn, and Wolfgang Von Der Linden. Spectral function of electron-phonon models by cluster perturbation theory. *Physical Review B*, 68(18):184304, November 2003.
 36. Mingu Kang, Sung Won Jung, Woo Jong Shin, Yeongsup Sohn, Sae Hee Ryu, Timur K. Kim, Moritz Hoesch, and Keun Su Kim. Holstein polaron in a valley-degenerate two-dimensional semiconductor. *Nature Materials*, 17(8):676–680, August 2018. Publisher: Nature Publishing Group.
 37. J. S. Zhou, R. Z. Xu, X. Q. Yu, F. J. Cheng, W. X. Zhao, X. Du, S. Z. Wang, Q. Q. Zhang, X. Gu, S. M. He, Y. D. Li, M. Q. Ren, X. C. Ma, Q. K. Xue, Y. L. Chen, C. L. Song, and L. X. Yang. Evidence for band renormalizations in strong-coupling superconducting alkali-fulleride films. *Phys. Rev. Lett.*, 130:216004, May 2023.
 38. L. J. P. Ament, M. Van Veenendaal, and J. Van Den Brink. Determining the electron-phonon coupling strength from Resonant Inelastic X-ray Scattering at transition metal L-edges. *EPL (Europhysics Letters)*, 95(2):27008, July 2011.
 39. S. Moser, S. Fatale, P. Krüger, H. Berger, P. Bugnon, A. Magrez, H. Niwa, J. Miyawaki, Y. Harada, and M. Grioni. Electron-phonon coupling in the bulk of anatase TiO_2 measured by resonant inelastic x-ray spectroscopy. *Physical Review Letters*, 115(9):096404, August 2015. Publisher: American Physical Society.
 40. S. Fatale, S. Moser, J. Miyawaki, Y. Harada, and M. Grioni. Hybridization and electron-phonon

- coupling in ferroelectric BaTiO₃ probed by resonant inelastic x-ray scattering. *Physical Review B*, 94(19):195131, November 2016. Publisher: American Physical Society.
41. Lucio Braicovich, Matteo Rossi, Roberto Fumagalli, Yingying Peng, Yan Wang, Riccardo Arpaia, Davide Betto, Gabriella M De Luca, Daniele Di Castro, Kurt Kummer, et al. Determining the electron-phonon coupling in superconducting cuprates by resonant inelastic x-ray scattering: Methods and results on Nd_{1+x}Ba_{2-x}Cu₃O_{7-δ}. *Physical Review Research*, 2(2):023231, 2020.
 42. David J. Abramovitch, Jin-Jian Zhou, Jernej Mravlje, Antoine Georges, and Marco Bernardi. Combining electron-phonon and dynamical mean-field theory calculations of correlated materials: Transport in the correlated metal Sr₂RuO₄. *Phys. Rev. Mater.*, 7:093801, Sep 2023.
 43. David J Abramovitch, Jernej Mravlje, Jin-Jian Zhou, Antoine Georges, and Marco Bernardi. Respective roles of electron-phonon and electron-electron interactions in the transport and quasiparticle properties of SrVO₃. *Physical Review Letters*, 133(18):186501, 2024.
 44. Y He, M Hashimoto, D Song, S-D Chen, J He, IM Vishik, B Moritz, D-H Lee, N Nagaosa, J Zaanen, et al. Rapid change of superconductivity and electron-phonon coupling through critical doping in Bi-2212. *Science*, 362(6410):62–65, 2018.
 45. Z. Wang, S. McKeown Walker, A. Tamai, Y. Wang, Z. Ristic, F. Y. Bruno, A. de la Torre, S. Riccò, N. C. Plumb, M. Shi, P. Hlawenka, J. Sánchez-Barriga, A. Varykhalov, T. K. Kim, M. Hoesch, P. D. C. King, W. Meevasana, U. Diebold, J. Mesot, B. Moritz, T. P. Devereaux, M. Radovic, and F. Baumberger. Tailoring the nature and strength of electron–phonon interactions in the SrTiO₃(001) 2D electron liquid. *Nature Materials*, 15(8):835–839, August 2016. Publisher: Nature Publishing Group.
 46. Chao Zhang, Feixiang Hao, Guanyin Gao, Xiang Liu, Chao Ma, Yue Lin, Yuewei Yin, and Xiaoguang Li. Enhanced superconductivity in TiO epitaxial thin films. *npj Quantum Materials*, 2(1):1–5, January 2017. Publisher: Nature Publishing Group.
 47. K. Yoshimatsu, O. Sakata, and A. Ohtomo. Superconductivity in Ti₄O₇ and γ-Ti₃O₅ films. *Scientific Reports*, 7(1):12544, October 2017. Publisher: Nature Publishing Group.
 48. ZV Popović, G De Marzi, MJ Konstantinović, A Cantarero, Z Dohčević-Mitrović, M Isobe, and Y Ueda. Phonon properties of the spinel oxide MgTi₂O₄ with the S= 1/2 pyrochlore lattice. *Physical Review B*, 68(22):224302, 2003.
 49. Paolo G Radaelli, Yoichi Horibe, Matthias J Gutmann, Hiroki Ishibashi, CH Chen, Richard M

- Ibberson, Yasumasa Koyama, Yew-San Hor, Valery Kiryukhin, and Sang-Wook Cheong. Formation of isomorphic Ir^{3+} and Ir^{4+} octamers and spin dimerization in the spinel CuIr_2S_4 . *Nature*, 416(6877):155–158, 2002.
50. Long Yang, Robert J Koch, Hong Zheng, JF Mitchell, Weiguo Yin, Matthew G Tucker, Simon JL Billinge, and Emil S Bozin. Two-orbital degeneracy lifted local precursor to a metal-insulator transition in MgTi_2O_4 . *Physical Review B*, 102(23):235128, 2020.
 51. M Capone, S Ciuchi, and C Grimaldi. The small polaron crossover: Role of dimensionality. In *Stripes and Related Phenomena*, pages 169–174. Springer, 2000.
 52. Misuzu Watanabe, Kazuhiro Kaneda, Hiroyuki Takeda, and Nobuo Tsuda. Semiconducting properties of $\text{Li}_{1.1}\text{Ti}_{1.9}\text{O}_4$. *Journal of the Physical Society of Japan*, 53(8):2437–2440, 1984.
 53. M. R. Harrison, P. P. Edwards, and J. B. Goodenough. A study of the $\text{Li}_{1+x}\text{Ti}_{2-x}\text{O}_4$ spinel system by diffuse reflectance spectroscopy. *Journal of Solid State Chemistry*, 54(3):426–437, October 1984.
 54. Shan Yang, A. T. Brant, N. C. Giles, and L. E. Halliburton. Intrinsic small polarons in rutile TiO_2 . *Physical Review B*, 87(12):125201, March 2013.
 55. S. Lakkis, C. Schlenker, B. K. Chakraverty, R. Buder, and M. Marezio. Metal-insulator transitions in Ti_4O_7 single crystals: Crystal characterization, specific heat, and electron paramagnetic resonance. *Physical Review B*, 14(4):1429–1440, August 1976. Publisher: American Physical Society.
 56. AR Davenport, JP Hague, and PE Kornilovitch. Mobile small bipolarons on a three-dimensional cubic lattice. *Physical Review B—Condensed Matter and Materials Physics*, 86(3):035106, 2012.
 57. JP Hague, PE Kornilovitch, JH Samson, and AS Alexandrov. Superlight small bipolarons in the presence of a strong coulomb repulsion. *Physical review letters*, 98(3):037002, 2007.
 58. Th Holstein. Studies of polaron motion: Part ii. the “small” polaron. *Annals of physics*, 8(3):343–389, 1959.
 59. R. T. Clay and D. Roy. Superconductivity due to cooperation of electron-electron and electron-phonon interactions at quarter filling. *Phys. Rev. Res.*, 2:023006, Apr 2020.